Vane Stagger Angle and Camber Effects in Fan Noise Generation

Johan B.H.M. Schulten*
National Aerospace Laboratory NLR, Amsterdam, the Netherlands

The problem of sound generated by the interaction of velocity disturbances with stator vanes in an annular duct is considered theoretically. The duct carries a uniform subsonic main flow and is assumed to be anechoic. In this problem it seems consistent to model the vanes by flat plates parallel to the duct axis. However, this modeling may yield an unrealistically low acoustic power. In the present paper, a nonplanar lifting surface approximation of the vanes shows that at frequencies prevailing in current turbofans even a small vane inclination significantly affects the sound generation process. The lower the circumferential periodicity $|m|$ of the cut-on sound field, the more pronounced are the acoustic effects of vane stagger angle and camber. Calculations for a typical example of a turbofan stator show at $|m| = 1$ a rise of 23 dB in upstream acoustic power when the stagger angle is increased from 0 to 15 deg. Furthermore, even at $|m| = 16$ there is still a rise of 5 dB. Besides the acoustic power, the modal distribution of the sound field is very sensitive to vane camber and stagger angle.

Nomenclature

$A_{n\mu}$ = pure tone modal pressure amplitude
$\boldsymbol{a}_{n\mu}(\alpha, r)$ = $(\alpha, -iU'_{n\mu}(r)/U_{n\mu}(r), n/r)$
$\boldsymbol{a}^*_{n\mu}(\alpha, \rho)$ = $(\alpha, iU'_{n\mu}(\rho)/U_{n\mu}(\rho), n/\rho)$
$\boldsymbol{b}_{n\mu}(x-\xi, r, \omega)$ = $\boldsymbol{a}_{n\mu}([\omega M - \mathrm{sgn}(x-\xi)\beta_{n\mu}]/\beta^2, r)$
$\boldsymbol{b}^*_{n\mu}(x-\xi, \rho, \omega)$ = $\boldsymbol{a}^*_{n\mu}([\omega M - \mathrm{sgn}(x-\xi)\beta_{n\mu}]/\beta^2, \rho)$
$\boldsymbol{c}_{n\mu}(r, \omega)$ = $\boldsymbol{a}_{n\mu}(-\omega/M, r)$
$\boldsymbol{c}^*_{n\mu}(\rho, \omega)$ = $\boldsymbol{a}^*_{n\mu}(-\omega/M, \rho)$
$\boldsymbol{F}$ = force field
$\boldsymbol{f}$ = force vector
G = Green's function
$\boldsymbol{g}(x, r)$ = $[-r(\partial\varphi_0/\partial x), -r(\partial\varphi_0/\partial r), 1]$, normal to vane surface
h = hub radius
$\boldsymbol{h}_{n\mu}$ = vector function defined by Eq. (12)
J = maximum j
j = radial wave number of Galerkin projection, vane index
k = circumferential wave number of disturbance velocity component
L = maximum ℓ
ℓ = axial wave number of Galerkin projection
M = mean flow Mach number
m = $k - nN$
N = number of vanes
$\boldsymbol{n}$ = unit normal on vane surface
n = integer number
$P_{k\eta\lambda}$ = pressure jump Fourier coefficient
p = pressure
$\Delta p_{k,0}$ = pressure jump across zeroth vane caused by kth disturbance velocity component
r = radial coordinate
t = time coordinate
$U_{n\mu}, U'_{n\mu}$ = radial eigenfunction, its derivative
$\boldsymbol{v}$ = velocity induced by the stator
$W, W_{n\mu}$ = pure tone total, modal power
$\boldsymbol{w}$ = disturbance velocity
x = axial coordinate
α = axial wave number
α_l = stagger angle at vane tip (Fig. 2)
β = $\sqrt{1-M^2}$
$\beta_{n\mu}$ = $\omega\sqrt{1-(\varepsilon_{n\mu}\beta/\omega)^2}$ if $(\varepsilon_{n\mu}\beta)^2 < \omega^2$; $-i\sqrt{(\varepsilon_{n\mu}\beta)^2-\omega^2}$ if $(\varepsilon_{n\mu}\beta)^2 > \omega^2$
γ_L = camber angle (see Fig. 2)
$\varepsilon_{n\mu}$ = modal eigenvalue
H = maximum η
η = radial wave number of pressure jump distribution
θ = angular coordinate
Λ = maximum λ
λ = axial wave number of pressure jump distribution
μ = radial mode index
ξ = axial source coordinate
ρ = radial source coordinate
τ = source time coordinate
φ = angular source coordinate
$\varphi_0(x, r)$ = angular coordinate of zeroth vane
ω = Helmholtz number [nondimensional radian frequency, (2π frequency × duct radius)/speed of sound]

Superscripts

$\tilde{(\ )}$ = in time domain
$\hat{(\ )}$ = axially Fourier transformed variable
$\bar{(\ )}$ = average over $[\xi - (x_T - x_L)/\Lambda, \xi + (x_T - x_L)/\Lambda]$
$(\ )^+$ = axially positive of source
$(\ )^-$ = axially negative of source

Subscripts

f = point force
L = leading edge
T = trailing edge

Other Symbols

$\langle \cdot \rangle$ = inner product of two three-dimensional vectors

Introduction

WITH the introduction of high-bypass turbofan engines into air transportation, the associated noise level was

Received March 18, 1983; presented as Paper 83-0766 at the AIAA Eighth Aeroacoustics Conference, Atlanta, Ga., April 11-13, 1983; revision received Oct. 18, 1983.

*Research Engineer, Department of Fluid Dynamics. Member AIAA.

substantially reduced. By this reduction the critical component in aircraft noise shifted from the jet to the fan, which still continues to be a major noise source. In a qualitative sense, the mechanism of subsonic fan noise generation is well known to be the interaction of nonaxisymmetric velocity disturbances from the rotor with the downstream stator. In general, these velocity disturbances comprise a variety of flow phenomena such as the trailing vortex system of the rotor, viscous wakes shed from the rotor blades, viscous-inviscid end-wall interactions, and rotor tip leakage.

In recent years the response of a blade row to velocity disturbances has been investigated theoretically by several researchers (Namba,[1] Kobayashi and Groeneweg,[2] Lordi and Homicz,[3] and Schulten[4]) by using three-dimensional lifting surface methods. Most of these studies[1-3] address the interaction of stationary velocity disturbances with a rotating blade row. In the usual linearized approach to the problem of evaluating the unsteady aerodynamic response, the rotor blades are then reduced to helical surfaces parallel to the mean relative flow in the rotating system. Kobayashi and Groeneweg[2] compared the acoustic power calculated from such a rotor model with the experimentally found power of a transonic fan. The velocity disturbances used in their experiment were the viscous wakes of stationary rods. In spite of the limitations in the model, the calculated acoustic power agreed remarkably well with the measured far-field power.

In practice, however, the fan noise is not generated at the rotor blades but at the stator vanes. Thus, it might appear that a stator could be considered as just a rotor with zero angular speed. Then the vanes reduce to flat plates parallel to the axial direction. This modeling was adopted in a previous study[4] to analyze the effect of vane lean. However, in routine calculations based on this stator model, a striking anomaly was found: the acoustic power varied strongly (up to the order of 15 dB) with the circumferential periodicity m of the acoustic field generated. At low $|m|$ values, unrealistically low power levels were obtained and it appeared that for a stator without lean the calculated power even vanished at $m = 0$.

In the present study it will be shown that taking into account the local vane surface inclination with respect to the main flow explains and resolves the above anomaly. This inclination inherently introduces *axial* vane force components that can be far more effective in sound generation than the circumferential components. In particular, at the high Helmholtz numbers (dimensionless frequencies) prevailing in current turbofan engines, the acoustic effects of such vane inclination are strong. At the same time, it will become clear why there is no need to consider a camber or an angle of attack in the modeling of a rotor. In that case, the main blade surface inclination is already determined by the helicoid defined by the rotational and axial velocities. Then inclusion of the local blade camber and stagger angle does not significantly alter the relative importance of axial and circumferential blade forces.

The present paper starts by constructing a mathematical model of a stator with cambered vanes at a stagger angle and exposed to an extraneous velocity field. This model will be cast in the form of an integral equation for the unknown pressure jump distribution over a single vane. Subsequently, the method of solving this equation will be described. Systematic numerical examples to quantify the effects of vane camber and stagger angle will be discussed in detail.

Analysis

Formulation of the Problem

The theoretical model consists of a single stator in an anechoic, hard-walled, annular duct. The duct carries an inviscid, uniform, subsonic main flow of Mach number M ($0 < M < 1$). Taking the duct radius and the mass density and sound speed of the main flow as scaling parameters, a *nondimensional formulation* will be used throughout. The x axis is chosen positive in the main flow direction along the duct axis (Fig. 1). Then the governing linearized equations for small, isentropic perturbations of the main flow read

$$\frac{\partial \tilde{p}}{\partial t} + M\frac{\partial \tilde{p}}{\partial x} + \nabla \cdot \tilde{v} = 0 \tag{1}$$

$$\frac{\partial \tilde{v}}{\partial t} + M\frac{\partial \tilde{v}}{\partial x} + \nabla \tilde{p} = \tilde{F} \tag{2}$$

The hard-wall boundary condition requires the normal velocity to vanish at the hub ($r = h$), casing ($r = 1$), and vanes. The presence of the vanes is accounted for via the external force field $\tilde{F}$ in Eq. (2), which will be identified later with the pressure jump across the vane surfaces. In addition, the perturbations generated by $\tilde{F}$ should radiate outward. This radiation condition relates to the energy flux vector. However, in the present problem, trailing vortex sheets are shed from the stator. In such a rotational flowfield, no definition of acoustic energy is possible because of the energy exchange between the main flow and the perturbations (see Rienstra[5]). Thus a radiation condition based on energy considerations cannot be formulated here and will be replaced by the condition of causality.

The vanes will be modeled as cambered surfaces of negligible thickness at a stagger angle and with a constant axial chord projection (Fig. 2). Vane thickness has been assumed to be negligible since the displacement of the flow by the vanes is a steady perturbation field. Interaction with the unsteady flowfield vanishes in the small perturbation limit considered here. The basic problem is to find the pressure jump distribution (PJD) that arises when the vanes are exposed to an extraneous velocity perturbation field. The PJD is accompanied by a countervelocity field, canceling the normal compo-

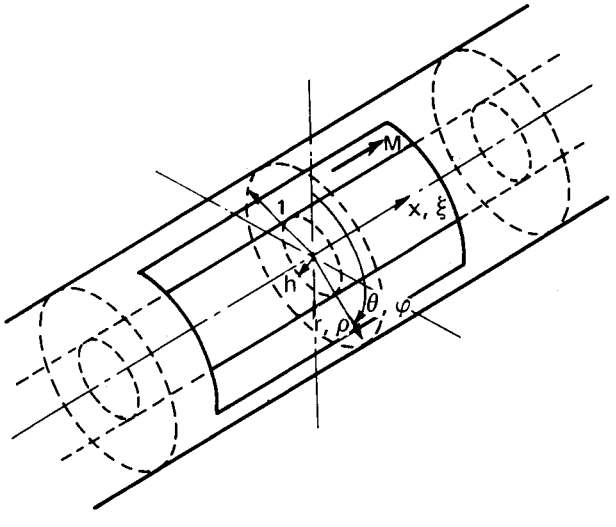

Fig. 1 Coordinate system.

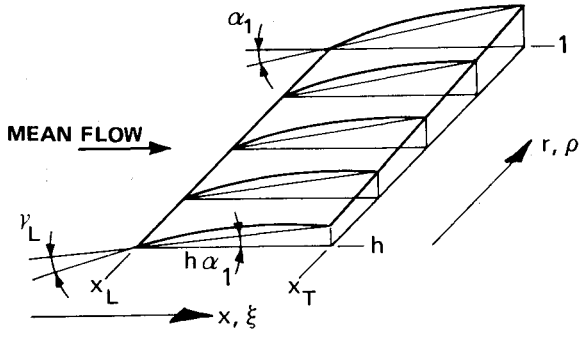

Fig. 2 Vane geometry, definition of the tip stagger angle α_1 and camber angle γ_L, $\alpha_1 = \gamma_L = 0.2$ (11.5 deg) shown.

nent of the extraneous velocities at the vanes. Based on this condition, an integral equation for the PJD will be derived in this section. Since inviscid flow is assumed, there is no unique solution of the PJD and a Kutta condition has to be added prescribing the flow behavior in the vicinity of the trailing edge of the vanes.

Field of a Point Force

By elimination of the velocity $\tilde{v}$ from Eqs. (1) and (2), the following inhomogeneous convected-wave equation for the pressure is obtained:

$$\left[\nabla^2-\left(M\frac{\partial}{\partial x}+\frac{\partial}{\partial t}\right)^2\right]\tilde{p}=\nabla\cdot\tilde{\boldsymbol{F}} \tag{3}$$

The standard way to solve this equation is first to construct the Green's function $\tilde{G}$ for the convected-wave operator and subsequently to find $\tilde{p}$ by integration over the vanes. The equation for $\tilde{G}$ is

$$\left[\nabla^2-\left(M\frac{\partial}{\partial x}+\frac{\partial}{\partial t}\right)^2\right]\tilde{G}$$

$$=-\delta(x-\xi)\delta(r-\rho)\frac{\delta(\theta-\varphi)}{r}\delta(t-\tau) \tag{4}$$

Upon Fourier transformation in t and x, assuming a Fourier-Bessel eigenfunction expansion in θ and r and utilizing the orthogonality of the eigenfunctions, it is found that

$$\tilde{G}=\left(\frac{1}{2\pi}\right)^3\int_{-\infty}^{\infty}\sum_{n=-\infty}^{\infty}\sum_{\mu=1}^{\infty}\int_{-\infty}^{\infty}\hat{G}_{n\mu}(\alpha,\omega|\xi,\rho,\varphi,\tau)$$

$$\times\exp(i\alpha x)\,\mathrm{d}\alpha\exp(in\theta)U_{n\mu}(r)\exp(i\omega t)\,\mathrm{d}\omega \tag{5}$$

where

$$\hat{G}_{n\mu}(\alpha,\omega|\xi,\rho,\varphi,\tau)=\frac{\exp[-i(n\varphi+\omega\tau+\alpha\xi)]U_{n\mu}(\rho)}{\varepsilon_{n\mu}^2+\alpha^2-(\omega+M\alpha)^2}$$

The homogeneous eigensolutions are omitted since they are not causal. The radial eigenfunctions $U_{n\mu}(r)$ are linear combinations of the Bessel functions $J_n(\varepsilon_{n\mu}r)$ and $Y_n(\varepsilon_{n\mu}r)$, such that both $U'_{n\mu}(h)=U'_{n\mu}(1)=0$. They are normalized to satisfy

$$\int_h^1 U_{n\mu}(r)U_{n\lambda}(r)r\,\mathrm{d}r=\delta_{\mu\lambda}$$

If the force field $\tilde{\boldsymbol{F}}$ in Eq. (3) is taken to be an impulsive force of amplitude $\boldsymbol{f}$ acting at the point (ξ,ρ,φ,τ), the same Fourier transform and Fourier-Bessel series expansion yield for the pressure field p_f

$$\hat{p}_{f,n\mu}(\alpha,\omega|\xi,\rho,\varphi,\tau)$$

$$=-i\langle\boldsymbol{a}^*_{n\mu}(\alpha,\rho)\cdot\boldsymbol{f}\rangle\hat{G}_{n\mu}(\alpha,\omega|\xi,\rho,\varphi,\tau) \tag{6}$$

where the vector $\boldsymbol{a}^*_{n\mu}(\alpha,\rho)=(\alpha,iU'_{n\mu}(\rho)/U_{n\mu}(\rho),n/\rho)$ results from the divergence operator in Eq. (3). After taking causality into account by properly positioning the poles relative to the complex contour of integration, the Fourier integral to α is performed analytically by summation of the residues. Being primarily interested here in frequency components of the field, the integration to ω will not be carried out. The resulting pressure field of the point force is given by

$$p_f(x,r,\theta,\omega|\xi,\rho,\varphi,\tau)=-\frac{1}{4\pi}\sum_{n=-\infty}^{\infty}\sum_{\mu=1}^{\infty}\frac{U_{n\mu}(r)U_{n\mu}(\rho)}{\beta_{n\mu}}$$

$$\times\exp\left[-i\omega\tau+in(\theta-\varphi)+i(x-\xi)\frac{\omega M-\mathrm{sgn}(x-\xi)\beta_{n\mu}}{\beta^2}\right]$$

$$\times\langle\boldsymbol{b}^*_{n\mu}(x-\xi,\rho,\omega)\cdot\boldsymbol{f}\rangle \tag{7}$$

The corresponding velocity field $\hat{\boldsymbol{v}}_f$ in the α domain is found in a similar way from the linearized momentum equation [Eq. (2)].

$$\hat{\boldsymbol{v}}_f(\alpha,r,\theta,\omega|\xi,\rho,\varphi,\tau)=\frac{1}{2\pi i}\sum_{n=-\infty}^{\infty}\sum_{\mu=1}^{\infty}\frac{\exp(in\theta)}{\omega+M\alpha}$$

$$\times U_{n\mu}(r)U_{n\mu}(\rho)\exp[-i(n\varphi+\omega\tau+\alpha\xi)]$$

$$\times\left\{\boldsymbol{f}-\frac{\langle\boldsymbol{a}^*_{n\mu}(\alpha,\rho)\cdot\boldsymbol{f}\rangle}{\varepsilon_{n\mu}^2+\alpha^2-(\omega+M\alpha)^2}\boldsymbol{a}_{n\mu}(\alpha,r)\right\} \tag{8}$$

where the vector $\boldsymbol{a}_{n\mu}(\alpha,r)=(\alpha,-iU'_{n\mu}(r)/U_{n\mu}(r),n/r)$ results from the gradient operator in Eq. (2).

Finally, the inverse Fourier transform ($\alpha\to x$) yields the velocity field of a point force

$$\boldsymbol{v}_f(x,r,\theta,\omega|\xi,\rho,\varphi,\tau)=\frac{\exp(-i\omega\tau)}{2\pi M}\sum_{n=-\infty}^{\infty}\exp[in(\theta-\varphi)]$$

$$\times\sum_{\mu=1}^{\infty}U_{n\mu}(r)U_{n\mu}(\rho)\left\{\exp\left[\frac{-i\omega}{M}(x-\xi)\right]\right.$$

$$\times\left[\boldsymbol{f}-\frac{\langle\boldsymbol{c}^*_{n\mu}(\rho,\omega)\cdot\boldsymbol{f}\rangle}{(\omega/M)^2+\varepsilon_{n\mu}^2}\boldsymbol{c}_{n\mu}(r,\omega)\right]H(x-\xi)$$

$$+\beta^2\frac{\exp\{i(x-\xi)[\omega M-\mathrm{sgn}(x-\xi)\beta_{n\mu}]/\beta^2\}}{2\beta_{n\mu}[\omega/M-\mathrm{sgn}(x-\xi)\beta_{n\mu}]}$$

$$\left.\times\langle\boldsymbol{b}^*_{n\mu}(x-\xi,\rho,\omega)\cdot\boldsymbol{f}\rangle\boldsymbol{b}_{n\mu}(x-\xi,r,\omega)\right\} \tag{9}$$

Field of a Stator

To obtain the field of a complete stator, we identify $\boldsymbol{f}$ with the force exerted by a small element of a vane surface during the time $\mathrm{d}\tau$. If the jth vane surface is given by $\varphi=\varphi_0(\xi,\rho)+j2\pi/N$ and its PJD by $\Delta\tilde{p}_j(\xi,\rho,\tau)$ we have

$$\boldsymbol{f}=\boldsymbol{g}(\xi,\rho)\,\Delta\tilde{p}_j(\xi,\rho,\tau)\,\mathrm{d}\xi\,\mathrm{d}\rho\,\mathrm{d}\tau \tag{10}$$

where

$$\boldsymbol{g}(\xi,\rho)=\left(-\rho\frac{\partial\varphi_0}{\partial\xi},-\rho\frac{\partial\varphi_0}{\partial\rho},1\right)$$

The summation over the blades can be explicitly performed by adopting the usual procedure to consider the stator response separately for every circumferential harmonic of the extraneous velocity disturbance field.[4] Then substitution of Eq. (10) into Eqs. (7) and (9), followed by integration over the source time τ and over the zeroth vane surface, yields the field of a stator exposed to a velocity disturbance field with circumferential periodicity k.

The resulting pressure is

$$p_k = -\frac{N}{4\pi}\sum_{n=-\infty}^{\infty}\exp(im\theta)$$
$$\times\sum_{\mu=1}^{\infty}\frac{U_{m\mu}(r)}{\beta_{m\mu}}\int_h^l\int_{x_L}^{x_T}\exp[-im\varphi_0(\xi,\rho)]$$
$$\times U_{m\mu}(\rho)\exp\{i(x-\xi)[\omega M-\mathrm{sgn}(x-\xi)\beta_{m\mu}]/\beta^2\}$$
$$\times\langle \boldsymbol{b}^*_{m\mu}(x-\xi,\rho,\omega)\cdot\boldsymbol{g}(\xi,\rho)\rangle\Delta p_{k,0}(\xi,\rho,\omega)\,\mathrm{d}\xi\,\mathrm{d}\rho \quad (11)$$

where $m=k-nN$. In Eq. (11) the modal amplitudes $A_{m\mu}$ can be readily identified as surface integrals over the zeroth vane.

The velocity is given by

$$\boldsymbol{v}_k = \frac{N}{2\pi M}\sum_{n=-\infty}^{\infty}\exp(im\theta)$$
$$\times\sum_{\mu=1}^{\infty}U_{m\mu}(r)\int_h^l\int_{x_L}^{x_T}\exp[-im\varphi_0(\xi,\rho)]$$
$$\times U_{m\mu}(\rho)\boldsymbol{h}_{m\mu}(x,r,\omega,\xi,\rho)\,\Delta p_{k,0}(\xi,\rho,\omega)\,\mathrm{d}\xi\,\mathrm{d}\rho \quad (12)$$

where $\boldsymbol{h}_{m\mu}$ is the expression within the large braces of Eq. (9) with $\boldsymbol{f}$ replaced by $\boldsymbol{g}(\xi,\rho)$ and n by m.

The local vane surface inclination with respect to the main flow is accounted for by the axial component of $\boldsymbol{g}(\xi,\rho)$, which is the tangent of the local inclination angle, see Eq. (10). In accordance with the assumption of small perturbations, this tangent is small compared to the circumferential component of $\boldsymbol{g}(\xi,\rho)$, i.e., unity. However, in the pressure [Eq. (11)] $\boldsymbol{g}(\xi,\rho)$ appears in an inner product. For a stator without vane lean, this inner product is

$$\langle \boldsymbol{b}^*_{m\mu}(x-\xi,\rho,\omega)\cdot\boldsymbol{g}(\xi,\rho)\rangle$$
$$=\frac{\mathrm{sgn}(x-\xi)\beta_{m\mu}-\omega M}{\beta^2}\rho\frac{\partial\varphi_0}{\partial\xi}+\frac{m}{\rho} \quad (13)$$

Thus, the axial component of $\boldsymbol{g}(\xi,\rho)$ is multiplied by the modal axial wave number. Now the most important part of the pressure field consists of propagating modes, i.e., with $\beta_{m\mu}$ real. For the first few of these, the upstream axial wave number is close to $-\omega(1+M)/\beta^2$ and the downstream wave number tends to $\omega(1-M)/\beta^2$. As a result, in Eq. (13) a small number (the local vane inclination, $\rho|\partial\varphi_0/\partial\xi|\ll 1$) is multiplied by a usually large number (ω, which is of the order of 50 in modern turbofan engines) to the effect that up to moderate m values the first term will already be dominant beyond a few degrees of inclination. Thus, only when $|m|\gg|\omega(\partial\varphi_0/\partial\xi)|$ is the axial component of the vane forces not important and can it be neglected. In the other case, the axial component is a very effective source of sound that is not to be ignored.

In the velocity [Eq. (12)] the inner product $\langle \boldsymbol{c}^*_{m\mu}\cdot\boldsymbol{g}\rangle$ appears as well as the above $\langle \boldsymbol{b}^*_{m\mu}\cdot\boldsymbol{g}\rangle$. This product has a similar magnifying effect on the influence of the axial component $\boldsymbol{g}(\xi,\rho)$. Thus, at frequencies relevant for fan noise, a small vane inclination brings about first-order changes in the kernels of both the modal pressure and velocity integrals and should not be neglected.

Finally, the boundary condition of the vanishing normal velocity is applied at the vane surfaces to obtain an integral equation for the PJD. If the circumferential Fourier component of the extraneous velocity disturbance field is given by $\boldsymbol{w}_k(x,r,\omega)\exp(ik\theta)$, the following equation for $\Delta p_{k,0}$ results:

$$\left\{\frac{N}{2\pi M}\sum_{n=-\infty}^{\infty}\exp[im\varphi_0(x,r)]\sum_{\mu=1}^{\infty}U_{m\mu}(r)\right.$$
$$\times\int_h^l\int_{x_L}^{x_T}\exp[-im\varphi_0(\xi,\rho)]U_{m\mu}(\rho)\langle \boldsymbol{n}(x,r)$$
$$\cdot\boldsymbol{h}_{m\mu}(x,r,\omega,\xi,\rho)\rangle\Delta p_{k,0}(\xi,\rho,\omega)\,\mathrm{d}\xi\,\mathrm{d}\rho$$
$$\left.=-\langle \boldsymbol{n}(x,r)\cdot\boldsymbol{w}_k(x,r,\omega)\rangle\exp[ik\varphi_0(x,r)]\right\}_{h<r<l}^{x_L<x<x_T} \quad (14)$$

Here $\boldsymbol{n}(x,r)$ is the unit normal vector of the zeroth vane surface. This vector is equal to $\boldsymbol{g}(x,r)/\|\boldsymbol{g}(x,r)\|$. Although not yet solved, the original boundary value problem has been reduced to finding the unknown PJD over a single bounded surface.

Solution Procedure

A first step toward the solution of $\Delta p_{k,0}(\xi,\rho,\omega)$ from Eq. (14) is its expansion into a suitable set of chordwise and spanwise basis functions. Here, the following truncated Fourier double series has been adopted

$$\Delta p_{k,0}(\xi,\rho,\omega)\approx\sum_{\eta=0}^{\mathrm{H}}\cos\left[\pi\eta\left(\frac{\rho-h}{l-h}\right)\right]$$
$$\times\sum_{\lambda=0}^{\Lambda}P_{k\eta\lambda}(\omega)\cos\left[\pi\lambda\left(\frac{\xi-x_L}{x_T-x_L}\right)\right] \quad (15)$$

As distinct from previous work,[4] the Glauert transformation to the axial coordinate in the series of Eq. (15) has been abandoned. Instead, the physical coordinate ξ is retained. The advantage of this is the possibility to perform the axial integration in Eq. (14) analytically after substitution of Eq. (15). On the other hand, the convergence of the series to the physical PJD will be rather slow ($\sim 1/\sqrt{\Lambda}$) because of the square root singularity of Δp to be expected at the leading edge. Furthermore, the truncated Fourier series expansion of this type of singularity oscillates about the expanded function with an axial periodicity mainly corresponding to the last term included (Λ). For Λ sufficiently large, the effects of such an oscillation cancel out in the pressure equation (11) and velocity equation (12) integrals.

However, just to obtain a physically relevant picture of the PJD, it is convenient to damp this oscillation by taking the average over the shortest axial wavelength $2(x_T-x_L)/\Lambda$ in the series. The resulting smoothed PJD is denoted by $\overline{\Delta p}(\xi,\rho,\omega)$. It is remarked that, for moderate values of Λ, the above averaging process masks a leading-edge singularity by representing it as a smooth and relatively wide bump. Thus, in the vicinity of the leading edge, $\overline{\Delta p}$ should be correctly interpreted.

Since the analysis leading to the governing integral equation (14) is for inviscid flow, the boundary condition of vanishing normal velocity is not sufficient for a unique PJD and an additional condition has to be imposed. In the present case, the usual, full Kutta condition has been adopted, which is equivalent to the requirement of no singular behavior of the PJD at the trailing edge, or $\Delta p\sim\sqrt{x_T-\xi}$ if $\xi\uparrow x_T$. Because the truncated series representing the PJD is subject to the nonphysical oscillatory behavior discussed above, the Kutta condition will be imposed on the smoothed PJD $\overline{\Delta p}(\xi,\rho,\omega)$ by requiring the parabolic behavior $(\partial/\partial\xi)\overline{\Delta p}/\overline{\Delta p}=$

$-\Lambda/[2(x_T-x_L)]$ at $\xi=x_T-(x_T-x_L)/\Lambda$. Substitution of the PJD expansion of Eq. (15) into this condition and using the orthogonality of the spanwise basis functions yields H + 1 linear equations for the coefficients $P_{k\eta\lambda}(\omega)$ ($\eta=0,1,\dots H, \lambda=0,1,\dots\Lambda$).

To solve the integral equation (14), the collocation method used in previous work[4] proved to be less attractive in the higher frequency range ($|\omega|>30$). It was found that the number of collocation points required for a well-converged solution very rapidly increases with increasing frequency, leading to large matrix systems. Since the matrix elements are rather time consuming to compute, an alternative method to solve the equation was adopted, namely a Galerkin projection method. For the present study, the following form of this method was used:

$$\int_h^1 \cos\left\{\pi j\left(\frac{r-h}{1-h}\right)\right\}\int_{x_L}^{x_T}\cos\left[\pi\ell\left(\frac{x-x_L}{x_T-x_L}\right)\right][\text{Eq. (14)}]\,dx\,dr$$
$$(j=0,1,2,\dots J, \ell=0,1,2,\dots L) \qquad (16)$$

After substitution of the Fourier series [Eq. (15)] into Eq. (14), Eqs. (16) turn into $(J+1)(L+1)$ linear algebraic equations. This set, completed by the H + 1 equations resulting from the Kutta condition, forms a system of equations in the unknown pressure jump coefficients $P_{k\eta\lambda}(\omega)$ ($\eta=0,1,\dots H, \lambda=0,1,\dots\Lambda$).

Obviously, the number of equations must be equal to the number of pressure jump coefficients, i.e., $(J+1)(L+1)=(H+1)\Lambda$. Upon truncation of the series in Eq. (14), the matrix elements of the system are computed using Namba's method[6] for the radial eigenfunctions of high m order. Finally, the system is solved by means of standard matrix techniques. For the acoustic quantities of interest, the above Galerkin method was found to be superior in convergence characteristics as compared to the collocation method. As a result the matrices could be kept within reasonable dimensions (100×100 for $|\omega|\sim50$). Of course, the Galerkin method itself is more laborious since an additional surface integration is required.

As is clear from Eqs. (14) and (16) the matrix elements result from a four-dimensional (ξ,ρ,x,r) integration that is repeated for each n,μ combination. About 200 of such combinations are typically required, which brings the total number of integrals to complete a 100×100 matrix up to the order of 2×10^6. This number was too high for routine computations and, therefore, it was worthwhile to look for possibilities to reduce the complexity of the integrals. To a certain extent, this is possible if the class of vane geometries considered is restricted and if, moreover, a distinction is made between the angular vane *displacement* and the *variable normal direction* over the vane surface. Both aspects of a nonplanar vane geometry appear in the governing equation (14). In that equation the φ_0 occurring in the function $\exp\{im[\varphi_0(x,r)-\varphi_0(\xi,\rho)]\}$ accounts for the angular displacement between the points (x,r) and (ξ,ρ) on the zeroth vane surface. On the other hand, derivatives of φ_0 are found in the vectors $\boldsymbol{g}(\xi,\rho)$ and $\boldsymbol{n}(x,r)$, representing the variable normal direction.

Now, a first reduction is obtained if the (ξ,ρ) surface integration in Eq. (14) and the (x,r) surface integration in Eqs. (16) simplify to products of the line integrals. To this end, the axial coordinates of leading and trailing edges have to be independent of the radial coordinate and the angular vane displacement relative to the leading edge, $\varphi_0(x,r)-\varphi_0(x_L,r)$, must depend only on the axial coordinate. Furthermore, to permit analytical (x,ξ) integrations, an angular displacement linear in (x,ξ) has been chosen in the present study. Thus, the *displacement* of the vane surface is approximated by

$$\varphi_0(x,r)-\varphi_0(x_L,r)=-\alpha_I(x-x_L) \qquad (17)$$

which is exact for an uncambered vane with a tip stagger angle α_I (Fig. 2). It is noted that Eq. (17) still includes the possibility of leaned vanes.

As distinct from the displacement, the φ_0 in the normal vectors $\boldsymbol{g}(\xi,\rho)$ and $\boldsymbol{n}(x,r)$ is not subject to severe restrictions to allow the separation of integrals mentioned above and an analytical (x,ξ) integration of Eqs. (16). For instance, any polynomial or trigonometric expansion of φ_0 in x,r suffices. To include the effect of camber on the variation of the normal direction in a straightforward way, a quadratic expression of φ_0 in x has been adopted (as far as φ_0 in $\boldsymbol{g}$ and $\boldsymbol{n}$ is considered). The amount of camber is characterized by the camber angle $\gamma_L(r)$, which represents the vane inclination at the leading edge relative to the chord line (see Fig. 2). Hence the derivatives occurring in the normal vectors $\boldsymbol{n}$ and $\boldsymbol{g}$ are given by

$$\frac{\partial\varphi_0}{\partial x}=-\alpha_I-\frac{\gamma_L(r)}{r}+\frac{2\gamma_L(r)(x-x_L)}{(x_T-x_L)r} \qquad (18a)$$

$$\frac{\partial\varphi_0}{\partial r}=\frac{\partial\varphi_0(x_L,r)}{\partial r}+\frac{(x-x_L)(x-x_T)}{x_T-x_L}\frac{\partial}{\partial r}\left[\frac{\gamma_L(r)}{r}\right] \qquad (18b)$$

A computer program based on the above solution procedure takes about 400 s of CPU time to run on a CDC Cyber 170-855 system for a typical case, including the matrix inversion. The inverse matrix is stored and the stator response to additional velocity disturbance profiles can be calculated in a few seconds of CPU time.

Numerical Results

Configurations

To investigate the effect of vane camber and angle of incidence a systematic numerical study was carried out. A stator of 80 vanes (no lean) with a constant chord of 0.1 duct radius was chosen as a representative example. A single frequency ($\omega=50$) velocity disturbance field was considered.

A Helmholtz number $\omega=50$ is a representative value for the second harmonic of the interaction noise in a practical engine (the first harmonic is usually designed to be cut off by proper selection of blade and vane numbers). The Helmholtz number of the second harmonic is given by 2 × (number of rotor blades times the tangential rotor tip Mach number). Thus, for example, $\omega=50$ may correspond to a rotor of 25 blades with unit tangential tip Mach number or, alternatively, to a rotor of 33 blades with a tip Mach number of 0.76. The circumferential wave number of the second harmonic of the rotor wake system is given by $k=2\times$ (number of rotor blades).

The analysis indicated that the circumferential periodicity m of the generated cut-on sound field determines the relative importance of vane inclination effects. Therefore, variation in m has been included by varying the circumferential periodicity k of the impinging velocity field in such a way that cut-on modes of $m=0,-1,-2,-4,-8$, and -16 result. At every k the (x,r) distribution of the impinging velocity was varied by taking five different (smooth) distributions of normal velocity [cf., Eq. (14)]. Since the acoustic effects of vane inclination were found to be quite similar for these five distributions, only the results of three of them will be discussed here, namely

$$-\langle\boldsymbol{n}(x,r)\cdot\boldsymbol{w}_k(x,r,\omega)\rangle\exp[ik\varphi_0(x,r)]$$
$$=1 \qquad \text{(upwash A)} \quad (19a)$$
$$=\cos\left[\pi\frac{x-x_L}{x_T-x_L}\right] \qquad \text{(upwash B)} \quad (19b)$$
$$=\cos\left[\pi\frac{r-h}{1-h}\right]\cos\left[\pi\frac{x-x_L}{x_T-x_L}\right] \qquad \text{(upwash C)} \quad (19c)$$

Physical and computational data for the numerical examples are summarized in Table 1.

Table 1 Physical and computational data

Number of stator vanes, N	80
Hub/tip ratio, h	0.46
Vane axial chord length, $x_T - x_L$	0.1
Axial Mach number, M	0.35
Helmholtz number, ω	50
Modal index, m $(= k - nN)$	$n(-10, -9, \ldots, 10)$
Modal index, μ	$\mu(1, 2, \ldots, 11)$
Chordwise expansion, $\Delta p_{k,0}$	$\Lambda = 13$
Spanwise expansion, $\Delta p_{k,0}$	$H = 6$
Axial Galerkin projections	$L = 12$
Radial Galerkin projections	$J = 6$
Number of radial integration steps	48

Pressure Jump Distribution

As explained in the analysis, the essential unknown in the problem is the PJD over the vanes. Once the PJD has been determined, the acoustic field in the duct can be readily calculated from Eqs. (11) and (12). Therefore, it is of interest to investigate to what extent the PJD is affected by vane camber and stagger angle. In Fig. 3 the PJD has been depicted in the form of the real and imaginary parts of the smoothed PJD, i.e., $\overline{\Delta p}_{k,0}$. The PJD is presented for a number of camber and stagger angles and two m values ($m = -1, -16$). The disturbance velocity field is upwash B [Eq. (19b)] at the vane surfaces.

Effect of Stagger Angle

The left-hand part of Fig. 3 shows the PJD for tip stagger angles $\alpha_1 = 0.2$ and 0.3 rad (11.5, 17.2 deg). The camber angle is taken to be zero in these cases. This means that the vane geometry is exactly covered by the present calculation model, both for the displacement and the normal direction. The middle of Fig. 3 gives the PJD corresponding to zero camber and stagger. It is seen that the PJD amplitudes at $m = -16$ are smaller than those at $m = -1$. At both $m = -1$ and -16 the real part of the PJD undergoes little variation. Only the radial waviness observed at $\alpha_1 = 0$ diminishes at the higher angles. The imaginary part of the PJD shows some variation in the aft tip region of the vane, while it is practically constant in the remaining area. It is remarkable that despite the radial uniformity of the upwash distribution the resulting PJDs are far from uniform. The smoothed leading-edge singularities are easily discernible.

Effect of Camber

The effect of camber on the PJD is depicted in the right-hand side of Fig. 3. Here the stagger angle has been taken to be zero. A marked difference is observed in the behavior of the PJD between $m = -1$ and -16. At $m = -1$ the amplitude of the PJD in the tip region grows progressively with the camber angle, resulting in a dramatic variation of shape and magnitude. At $m = -16$ the behavior is completely different: only a very moderate and gradual amplification of the PJD is observed, while the global shape is almost perfectly retained. Figure 3 also shows that the radial waviness of the PJD is damped by an increasing camber angle, in a way similar to the damping caused by an increasing stagger angle.

A possible reason for the steep rise of the PJD at $m = -1$ could be the chordwise interference due to the variation of the axial component of the normal direction: this variation is absent in the case of a pure stagger angle. From the analysis, it is known that in cases where the circumferential periodicity of the cut-on modes is low, the contributions of the axial forces dominate in the propagating field. With a parabolic camber, the axial component of the normal necessarily has its extreme values at leading and trailing edges. At the frequency $\omega = 50$ of the present examples, the axial wavelength of the dominating acoustic modes is about one chord length for the upstream

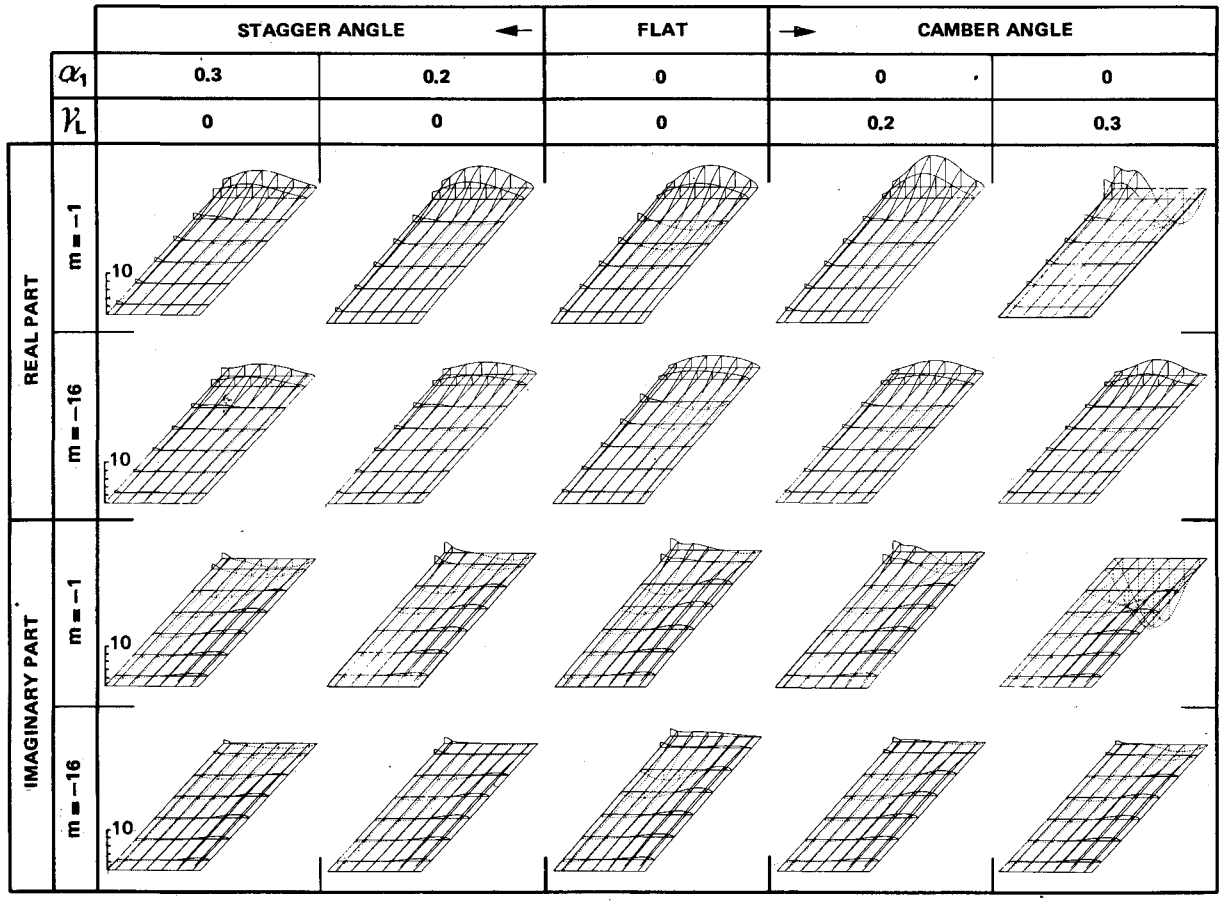

Fig. 3 Smoothed pressure jump distribution $\overline{\Delta p}_{k,0}$ over zeroth vane when exposed to upwash B [Eq. (19b)], conditions in Table 1.

propagating waves and about two chord lengths for the downstream waves. Furthermore, the hydrodynamic wavelength is on the order of half a chord. These wavelengths make a coupling with the camber plausible. Nevertheless, the observed rise of the PJD is remarkably strong. In this regard, it is noteworthy that a high $|m|$ is very effective in suppressing the sudden PJD rise.

It is to be noted that the effect of camber at $m = -4$ is practically the same as at $m = -1$. Application of other upwash distributions shows a similar behavior of the PJD with respect to camber.

Acoustic Effects

The PJD over the vanes is the key to the present physical problem. However, in an acoustical context, the generated sound field is of more practical interest. Therefore, the upstream $(\ )^-$ and downstream $(\ )^+$ pure tone acoustic power of the sound field will be discussed. Also the modal distribution of the cut-on sound field will be considered.

Following Morfey,[7] but ignoring the extraneous velocity field and trailing vortices, the pure tone modal power $W_{m\mu}$ emitted outward from the stator is given by

$$W^{\pm}_{m\mu} = \frac{\beta^4 \beta_{m\mu} |A^{\pm}_{m\mu}|^2}{\pi\omega\left(1 \mp \frac{M\beta_{m\mu}}{\omega}\right)} \quad \text{if } \beta_{m\mu} \text{ is real (cut-on)}$$

$$= 0 \quad \text{if } \beta_{m\nu} \text{ is imaginary (cut-off)} \quad (20)$$

where $A_{m\mu}$ is now understood to be the pure tone modal amplitude. Per frequency, the total acoustic power is the sum of the modal powers. In the present case, there is only one pure tone ($\omega = 50$).

m Effect

In Fig. 4 the acoustic power has been plotted as a function of the circumferential periodicity m of the cut-on sound field generated by a uniform upwash A and a double-cosine upwash C [Eqs. (19)]. Computed results of two vane geometries are shown: a flat vane parallel to the mean flow ($\alpha_l = 0$) and an uncambered, helical vane with 5.7 deg tip stagger angle ($\alpha_l = 0.1$). Although this is only a small angle compared to practical values, the effect in acoustic behavior is already remarkable. At $m = -1$ there is a power difference on the order of 15 dB. At $m = 0$ the modal amplitudes, and hence the acoustic power, *vanish* for $\alpha_l = 0$. It is noted that there is virtually no difference in the PJD at $\alpha_l = 0$ and $\alpha_l = 0.1$ for all m investigated. This emphasizes the *acoustic* significance of vane inclination.

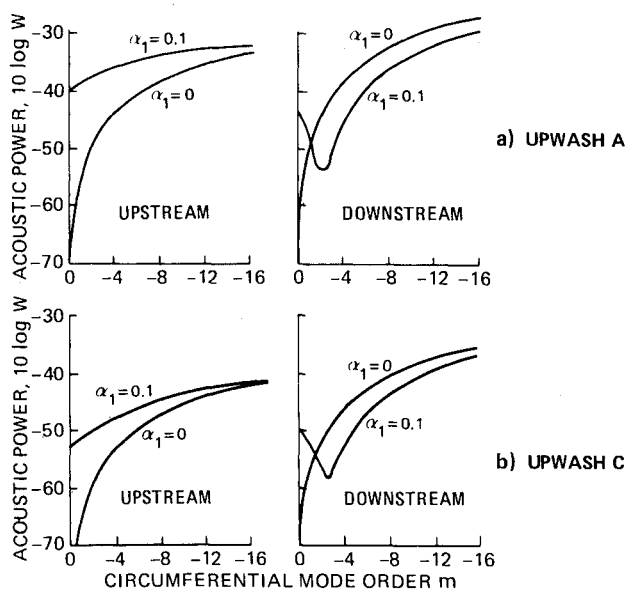

Fig. 4 Acoustic power as a function of the circumferential periodicity m of the cut-on modes for zero ($\alpha_l = 0$) and 5.7 deg ($\alpha_l = 0.1$) vane tip stagger angle (no camber, further conditions in Table 1).

For both upwash distributions the power variation is similar. As $|m|$ increases the power difference decreases, but remains significant in three out of the four cases shown. The minimum in the downstream power is caused by the opposing contributions to the modal amplitudes by the axial and circumferential forces [see Eq. (13)]. If the circumferential periodicities k of the impinging velocity field had been such that cut-on sound fields of positive m were generated, then such a minimum would have been expected in the upstream power. Since the axial wave number of the upstream cut-on modes is about twice the downstream wave number, the minimum then would be found at an $|m|$ value lower than for the downstream power.

Stagger Angle Effects

Figure 5 gives the acoustic power as a function of the tip stagger angle of an uncambered vane exposed to a uniform upwash as the driving velocity field. The circumferential periodicities of this velocity field have been chosen such that cut-on modes with $m = -1$, -4, and -16 are generated. Upstream of the stator, a very regular power variation is observed; the power increases with α_l and $|m|$. Even at $m = -16$ there is still a significant rise of 5 dB in the acoustic power as α_l is increased from 0 to 15 deg.

The downstream power exhibits quite different behavior. This is attributable to the opposing contributions of axial and circumferential forces mentioned above. For $m = -4$ a clear minimum results. For $m = -1$ the minimum practically coincides with zero angle of incidence, whereas for $m = -16$ the minimum is beyond 17 deg.

Camber Effects

It has already been found that, in contrast to a stagger angle, the camber has a large effect on the PJD if $|m|$ is low. Thus, it is to be expected that the effect of camber on the acoustic power will also be large. In Fig. 6 the acoustic power is plotted as a function of the camber angle (γ_L) for a uniform upwash. Here the contrast between high and low $|m|$ values is even more pronounced than for the stagger angle effects. For $m = 1$ the upstream acoustic power rises as much as 30 dB if the camber angle is increased from 0 to 15 deg. On the other hand, the $m = -16$ sound field shows a practically constant acoustic power over the same range.

The most interesting point, however, is that the $m = -1$ and -4 sound fields become more powerful than the $m = -16$ field beyond a certain relatively small camber angle. This behavior was also found for other upwash distributions. It is

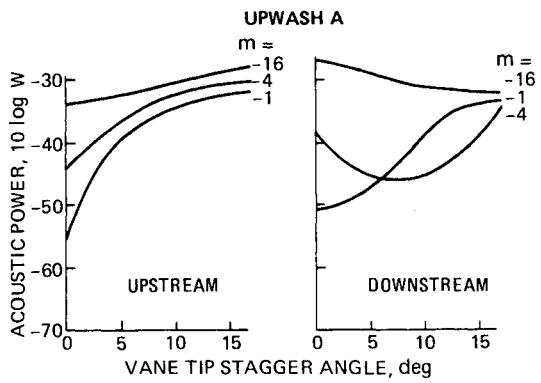

Fig. 5 Acoustic power as a function of the stagger angle of the vanes (uniform upwash, no camber, further conditions in Table 1).

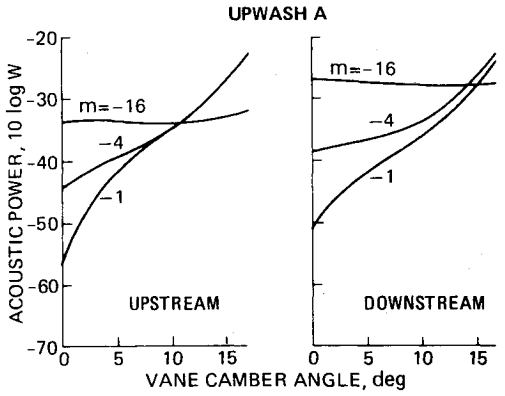

Fig. 6 Acoustic power as a function of the vane camber angle (uniform upwash, zero stagger angle, further conditions in Table 1).

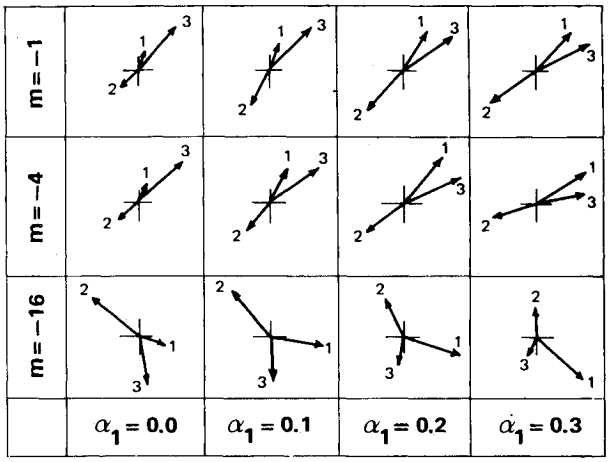

Fig. 7 Effect of stagger angle on modal distribution, complex plane representation of modal amplitudes ($\mu = 1,2,3$) at upstream station $x = x_L - 0.4$ (for each triad of vector the origin at the center, uniform upwash, no camber, further conditions in Table 1).

noted that 15 deg is still a modest camber angle, since angles on the order of 40 deg are common in practice. The phenomenon observed indicates a tendency for high $|m|$ fan designs to be more quiet. Of course, in practice nonlinearities may play an interfering role, but the present effect is so strong that it may offer an unexpected possibility to minimize fan noise by selecting high $|m|$ values.

Modal Distribution

Thus far the sound field has been characterized by its acoustic power. Although power is the most relevant global quantity, it does not contain information on the (complex) amplitudes of the cut-on modes that define the shape of the propagating sound field and are crucial to the possibilities of attenuation by duct lining.

To see how the modal distribution is affected by vane inclination the first three radial modes ($\mu = 1,2,3$) at $m = -1$, -4, and -16 were plotted for a number of stagger and camber angles. The complete cut-on field consists of 10 radial modes at $m = -1$ and -4, and 9 radial modes at $m = -16$. In the present numerical examples, however, the low μ-order modes usually dominate and yield a reasonable approximation of the complete field. Figure 7 gives a typical example of the development of the modal composition as the stagger angle is increased. Since tremendous differences in magnitude resulted for different m and stagger angles, each set of modal amplitudes had to be scaled to obtain similarly sized plots. The resulting relative magnitude of the modal amplitudes is to be compared only within each triad of vectors. From Fig. 7 it is obvious that at all three m levels the modal distribution changes significantly over a range of 17 deg of stagger. It is remarkable that the modal distribution at $m = -16$ varies as rapidly as in the lower $|m|$ cases.

It was found that variation of the camber angle causes changes of similar magnitude in the modal distribution. Thus, it is concluded that vane inclination plays an essential role not only in the acoustic power but also in the modal distribution of the field.

Conclusions

A three-dimensional lifting surface theory to calculate the sound field produced by a stator with nonplanar vanes exposed to unsteady velocity disturbances has been formulated. It has been shown that, at the high frequencies prevailing in current turbofan engines, the effects of vane camber and stagger angle are essential. Even a small axial component in the vane force distribution makes a significant contribution to the kernels of the pressure and velocity integrals of the problem. This contrasts with a rotor, for which in a small-perturbation approach the blades can correctly be reduced to helical surfaces parallel to the relative mean flow. Under certain restrictions on the vane stagger angle and camber distribution for computational efficiency, the resulting integral equation for the pressure jump distribution (PJD) is solved by a Galerkin projection method.

At a frequency typical for the second harmonic of a turbofan engine ($\omega = 50$), the effects of vane camber and stagger angle were studied numerically. From this numerical investigation the following conclusions are drawn:

1) Since five different upwash distributions all yielded similar aerodynamic and acoustic behavior, it is concluded that the observed phenomena do not depend essentially on details of the velocity field impinging on the stator.

2) The variation of the PJD with the stagger angle is gradual for both low and high $|m|$ values.

3) For small m values ($|m| < 4$), the PJD shows a spectacular nonlinear change in magnitude and shape when the camber angle is increased beyond about 10 deg. At $m = -16$ the PJD exhibits only minor variation over a range of 0-17 deg of camber angle.

4) For a given stagger angle α_l of the vanes, the acoustic power generally increases with $|m|$. However, for small values of α_l ($\alpha_l \sim 0.1$ rad), either the upstream or downstream power (depending on the sign of $m\alpha_l$) has a minimum. The smaller α_l, the steeper is the power variation with m.

5) The effect of vane camber on acoustic power strongly depends on the m value of the sound field. At $m = -16$ both the upstream and downstream power are practically constant over the camber angle range investigated (0-17 deg). At low $|m|$ values, however, the power increases very rapidly with increasing camber angle (up to 30 dB over 15 deg). As a result, beyond a relatively small camber angle (10-15 deg), a low $|m|$ sound field ($|m| < 4$) becomes more powerful than an $m = -16$ field. This indicates a possibility of high $|m|$ fan designs to be quieter for a practical camber angle.

6) Apart from their effect on the acoustic power, vane camber and stagger angle significantly affect the modal composition, i.e., the shape of the sound field. Also, in cases where the acoustic power is fairly constant, the individual modal amplitudes may show considerable variation.

Acknowledgments

The present investigation was sponsored by the Netherlands Agency for Aerospace Programs (NIVR). The computer programming was skillfully performed by C.H. Hofstra. The author is indebted to Dr. S.W. Rienstra for many helpful discussions and valuable advice.

References

[1]Namba, M., "Three-Dimensional Analysis of Blade Force and Sound Generation for an Annular Cascade in Distorted Flows," *Journal of Sound and Vibration*, Vol. 50, No. 4, 1977, pp. 479-508.

[2]Kobayashi, H. and Groeneweg, J.F., "Effects of Inflow Distortion Profiles on Fan Tone Noise," *AIAA Journal*, Vol. 18, Aug. 1980, pp. 899-906.

[3]Homicz, G.F., Lordi, J.A., Ludwig, G.R., Nenni, J.P., and Erickson, J.C., "Investigations of Rotating Stall Phenomena in Axial Flow Compressors, Vol. II: Investigation of Rotor-Stator Interaction Noise and Lifting Surface Theory for a Rotor," AFAPL-TR-76-48, June 1976.

[4]Schulten, J.B.H.M., "Sound Generated by Rotor Wakes Interacting with a Leaned Vane Stator," *AIAA Journal*, Vol. 20, Oct. 1982, pp. 1352-1358.

[5]Rienstra, S.W., "A Small Strouhal Number Analysis for Acoustic Wave-Jet Flow-Pipe Interaction," *Journal of Sound and Vibration*, Vol. 86, No. 4, 1983, pp. 539-556.

[6]Namba, M., "Lifting Surface Theory for a Rotating Subsonic or Transonic Blade Row," British Aeronautical Research Council, R&M 3740, Nov. 1972.

[7]Morfey, C.L., "Sound Generation in Ducts with Flow," *Journal of Sound and Vibration*, Vol. 14, No. 1, 1971, pp. 37-55.